Vol. 14, No. 4, 2023
ISSN 2233-4203/ e-ISSN 2093-8950
ARTICLE www.msletters.org | Mass Spectrometry Letters

Generation of Water Droplet Ion Beam for ToF-SIMS Analysis

Myoung Choul Choi[1], Ji Young Baek[1], Aram Hong[1], Jae Yeong Eo[2], and Chang Min Choi[1]*

[1]*Center for Scientific Instrumentation, Korea Basic Science Institute, Cheongju, Republic of Korea*
[2]*Center for Research Equipment, Korea Basic Science Institute, Cheongju, Republic of Korea*

Received September 19, 2023, Revised November 5, 2023, Accepted November 10, 2023
First published on the web December 31, 2023; DOI: 10.5478/MSL.2023.14.4.147

Abstract : The increasing demand for two-dimensional imaging analysis using optical or electronic microscopic techniques has led to an increase in the use of simple one-dimensional and two-dimensional mass spectrometry imaging. Among these imaging methods, secondary-ion mass spectrometry (SIMS) has the best spatial resolution using a primary ion beam with a relatively insignificant beam diameter. Until recently, SIMS, which uses high-energy primary ion beams, has not been used to analyze molecules. However, owing to the development of cluster ion beams, it has been actively used to analyze various organic molecules from the surface. Researchers and commercial SIMS companies are developing cluster ion beams to analyze biological samples, including amino acids, peptides, and proteins. In this study, a water droplet ion beam for surface analysis was realized. Water droplets ions were generated via electrospraying in a vacuum without desolvation. The generated ions were accelerated at an energy of 10 keV and collided with the target sample, and secondary ion mass spectra were obtained for the generated ions using ToF-SIMS. Thus, the proposed water droplet ion-beam device showed potential applicability as a primary ion beam in SIMS.

Keywords : Mass Spectrometry imaging, ToF-SIMS, Primary ion beam, Water droplet ion beam

Introduction

Mass spectrometry imaging (MSI) is an effective surface analysis technique because it can obtain a mass spectrum from each pixel to represent the components of a surface in two dimensions. This analytical method effectively observes the surface and can simultaneously probe various molecular ions along the x–y plane. Therefore, contrary to conventional optical microscopic techniques, it provides chemical information, which can mostly delineate visible morphology.[1–3] Electron microscopy can also give chemical information from a surface sample; however, it provides the elemental distribution but not molecular ion distribution, by using energy dispersive X-ray analysis (EDX) in scanning electron microscopy (SEM)[4,5] and electron energy-loss spectroscopy (EELS) in transmission electron microscopy (TEM).[6–8]

*Reprint requests to Chang Min Choi
https://orcid.org/0000-0002-3594-7881
E-mail: cmchoi@kbsi.re.kr

MSI possessing these advantages can be represented by three methods: desorption electrospray ionization (DESI)-MS,[9,10] matrix-assisted laser desorption ionization (MALDI)-MS,[11–13] and secondary-ion mass spectrometry (SIMS).[14–16] Each method has its own advantages and disadvantages from an imaging mass spectrometric perspective. The analysis method can be determined based on the subject of the analysis, approach adopted, and time required. DESI involves spraying a solvent droplet onto a sample surface to desorb ions at atmospheric pressure. The ions produced by a highly charged droplet were introduced into a mass spectrometer to analyze the chemical information on the surface. Mass spectrometry was performed along the x–y direction by moving a stage to reconstruct a two-dimensional MSI. DESI is a powerful surface analysis method for measuring atmospheric pressure and does not require sample preparation. However, reducing the minimum radius of solvent spraying to under 20 μm is challenging, and this strongly relates to image resolution.

MALDI can generate ions from coexisting matrix molecules and analytes in a sample via irradiation with an ultraviolet (UV) laser in vacuum. As the sample stage moves, MALDI expresses the mass spectral image as a two-dimensional distribution of molecular ion signals. MALDI can achieve better image resolution than DESI because it can reduce the minimum radius of the laser beam to below 5 μm. However, MALDI requires more sample preparation time than DESI and must be analyzed in vacuum. Therefore, only relatively dead biological samples can be analyzed. For both of these methods, the movement

of the sample stage for high-resolution MSI must be accurately controlled.

SIMS with a high-energy primary ion beam has been used to analyze monoatomic and diatomic ions sputtered from the sample surface. The kinetic energy of the primary ion beam is too high to ionize or observe intact molecular ions. However, cluster ion beams enhance molecular ion detection, enabling effortless application in bioimaging mass spectrometry through time-of-flight secondary ion mass spectrometry (ToF-SIMS). Because the gas cluster ion beam (GCIB) was developed, it enhanced molecular ion observation because the energy per nucleus was softly reduced to desorb and ionize ions.[17] Moreover, secondary molecular ions with less fragmentation must be detected using GCIB because it is a powerful instrument for analyzing molecular ions on surfaces. Among the various cluster ion beams, GCIB is the most widely used for biological sample and organic molecule analyses. John et al. used GCIB to ionize biomolecules, such as lipids, and analyzed the biological images of tissues.[18,19]

Thus, the primary ion beam contributes significantly to the performance of MSI through improved ionization in SIMS. However, the analysis of biomolecules, such as proteins, by using SIMS remains challenging. Therefore, there have been attempts to develop a GCIB using reactive gas to increase the ionization efficiency of biomolecules and analyze them.[20] Hua et al. recently published research results on biomolecules, such as proteins, using a 70 keV water cluster ion beam and ToF-SIMS.[21] Ninomiya et al. developed a vacuum-type electrospray droplet impact (V-EDI) to improve the secondary ionization yield by impacting water droplets containing numerous protons on the surface.[22]

This study developed a primary ion beam with high secondary ionization yield, aiming to have a significant impact on MSI surface analysis. Additionally, a water droplet was formed using a beam instrument similar to that developed by Ninomiya et al. The performance of the constructed primary ion beam determined its applicability as an ionization source for secondary ion mass spectrometry. Furthermore, it was coupled with a home-built ToF-SIMS to analyze the secondary molecular ions generated on the surface.

Experimental

Sample preparation

A 10 mm × 10 mm stainless-steel plate was used as the substrate to produce all monolayer microfilms. The substrates were ultrasonically cleaned in ethanol and distilled water for 10 min and thoroughly rinsed in deionized water. The chemically cleaned stainless steel substrates were dried using N_2 gas. Rhodamine 6G and bradykinin were purchased from Sigma-Aldrich and were used without further purification. The thin organic molecular film was prepared on a clean stainless steel plate by spin-coating (3000 rpm) approximately 1 mM aqueous solution (10 μL).

Instrument

The experimental setup for V-EDI is shown in Figure 1. Furthermore, it consisted of one chamber divided into two parts. The first part contained the electrospray, and the second part contained the ion optics, including the electrostatic lens. A turbomolecular pump (HiPace 80, Pfieffer Vacuum, Germany) was installed in the first part to maintain vacuum, and the second part was connected to the sample chamber of the secondary ion mass spectrometer to maintain vacuum. A 0.01 M TFA ethanol aqueous solution (ethanol:water = 1:4) was used as the liquid source of V-EDI. The syringe pump (Legato 110, KD Scientific) transferred the acidic ethanol aqueous solution to the source chamber through a PEEKSIL tubing (ID 150 μm, IDEX, USA). We tried to find the condition which the TFA ethanol aqueous solution would flow out uninterruptedly under the vacuum. It was confirmed that water droplets were continuously formed on the electrospray emitter at a flow rate of 1.5 μL/min, and a faster flow rate affected the vaccum state by supplying too much sovelnt. Therefore, a water droplet ion beam was generated at this flow rate. The electrospray emitter used in this study was the sharp singularity emitter (ID 2 μm, Fossil

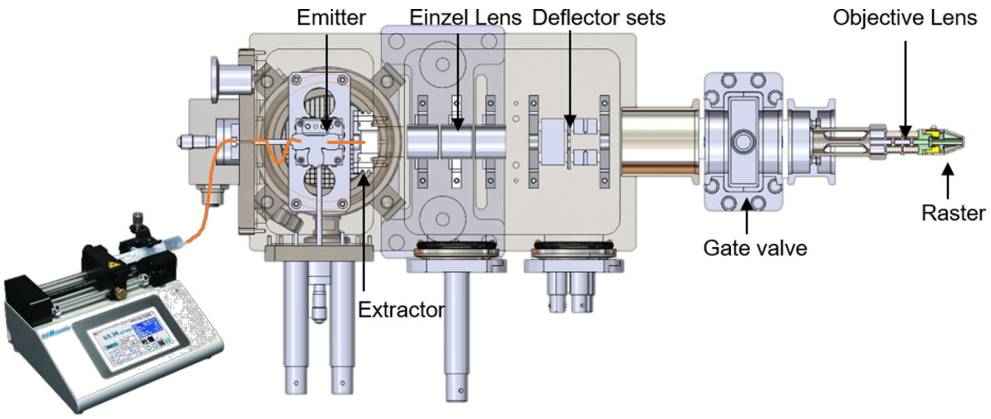

Figure 1. Schematic diagram for the experimental setup of the water droplet ion beam.

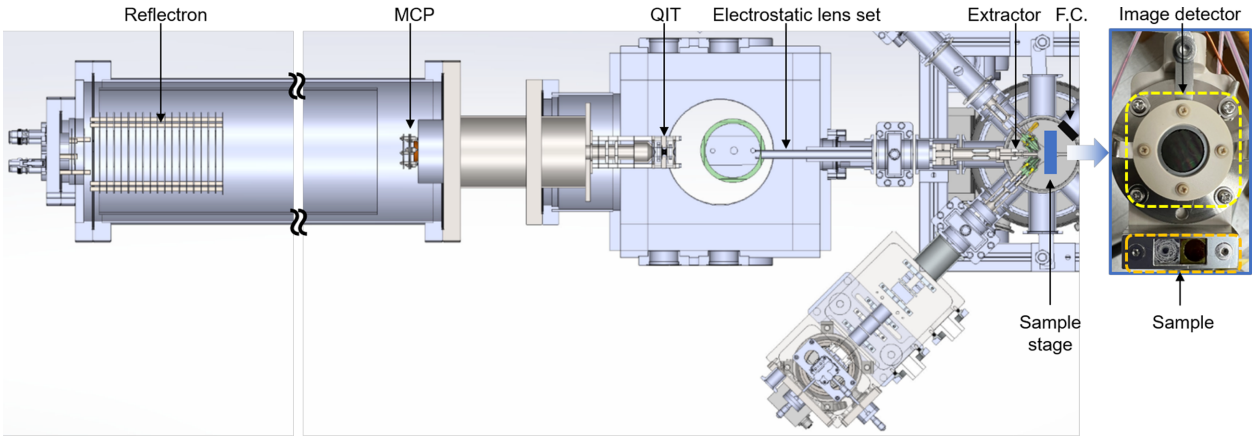

Figure 2. Schematic diagram for the homebuilt quadrupole iontrap time-of-flight secondary ion mass spectrometer and the photograph of a sample stage including an image detector.

Ion Tech, Madrid, Spain). The PEEKSIL tubing was connected to an electrospray emitter inside a microtee (P-885, IDEX), where a platinum wire, which floated to a high voltage (HV), was also inserted perpendicularly to both the tubing and the emitter. The droplets passing through the extractor were spatially focused by an Einzel lens, and the final focusing was performed using the objective lens installed at the end. A two-stage deflection electrode set that can deflect the ion beam was installed between the two lenses, and a raster electrode was installed at the end of the objective lens to scan the ion beam. Additionally, to prevent freezing of the liquid in the vacuum, the end of the electrospray emitter was irradiated by a continuous wave (CW) near-IR laser module (λ = 808 nm, 1.2 W, CivilLaser, China). In order to locally heat the electrospray emitter using a laser, the laser was preheated for more than 20 minutes before irradiating the laser, and the power was set to 400 mW using a lser power meter.

Experimental analyses

A Faraday cup was installed opposite the ion beam in the sample chamber to measure the output of the ion beam, and an image detector, including an MCP and a phosphor screen (F2221-11P-Y005, Hamamatsu Photonics, Japan), was installed on the sample stage to check the size of the ion beam. The total water droplet ion beam current was measured with a Faraday cup and monitored using a picoammeter (6485, Keithley, USA). The image of the water droplet ion beam on the phosphor screen was directly observed using a webcam (C920, Logitech, Switzerland). Sample analysis was performed using a home-built quadrupole ion trap reflectron–time-of-flight mass spectrometer (QIT-ToF-SIMS; see Figure 2). The sample stage mounted on the xyz manipulator was lowered to block the primary ion beams produced by V-EDI. Water droplet ions are accelerated to the sample stage to generate secondary ions. Therefore, the secondary ions sputtered by the 10 keV water droplet ion projectiles were accelerated to QIT-ToF-SIMS at 100 VDC. The secondary ions enter the QIT through a set of extraction and electrostatic lenses. To enhance the sensitivity and perform ToF-SIMS analysis, a radio frequency signal of constant frequency and amplitude was applied to the ring electrode with both end-caps grounded, where most of the secondary ions can be stored. Next, a positive DC pulse was applied to the entrance end cap to extract all the ions in the QIT to a reflectron ToF-SIMS for mass analysis. The ions were reflected by a reflectron and detected using a 40 mm dual microchannel plate (MCP). Ion signals from the MCP were processed using a digital storage oscilloscope. The timings of ion storage, extraction, and detection were synchronized using TTL pulses from a digital delay generator. A secondary ion mass spectrum was obtained in the positive mode using a 10 keV water droplet ion as the analysis ion beam.

Results and Discussion

Figure 3 shows photographs of the electrospray phenomena (a) under atmospheric pressure and (b) in vacuum. As shown in Figure 3 (a), two lasers were irradiated in front of the emitter to observe the light scattering from the water droplets produced by the electrospray. Figure 3 (a) shows an electrospray plume. Furthermore, the plume size was drastically broadened by dispersion in the air immediately after spraying at atmospheric pressure. However, it was not widely sprayed in a vacuum, which was similar to that reported by Ninomiya et al.[23] Compared to electrospray under atmospheric pressure, electrospray in vacuum is effortless to maintain linearity because there are fewer multiple collisions with the air at the center of the trajectory. However, this can enhance the current and brightness of the ion beam compared to atmospheric-pressure-type electrospray droplet impact (A-VDI), indicating that a V-EDI source was successfully generated.

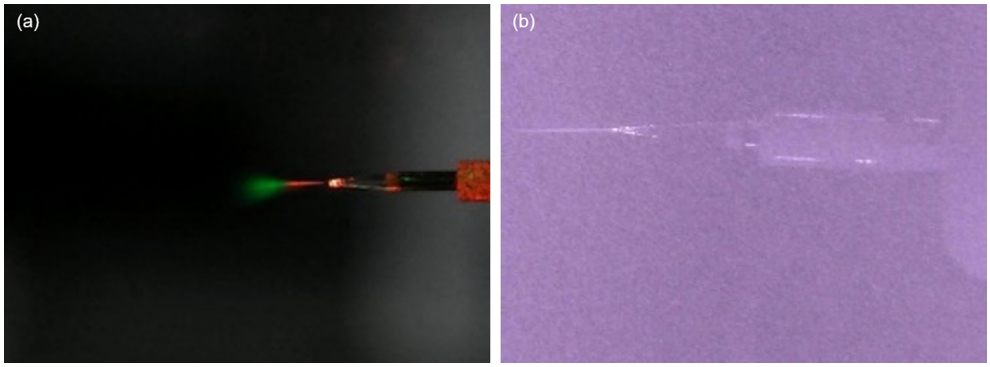

Figure 3. Photographs of an electrospray (a) in the atmospheric pressure and (b) in the vacuum.

A Faraday cup was installed to measure the current of the water droplet ion beam. Figure 4 shows the current as a function of time, and the inset in Figure 4 shows a photograph of the picoammeter used to measure the current of the water droplet ion beam. Except in cases where the current of the water droplet ion beam was high when the ion beam was emitted at the start, the current was maintained at an average of approximately 2.3 nA for 1 h. The fluctuation in current was because of an unstable supply of high voltage, electrical discharge, or inconsistent supply of solution, which is the flow of the solution. However, the stability of the currently used high-voltage power source for ion beams is approximately 0.05 %, which cannot be considered owing to fluctuations in the output due to voltage. In addition, if there was a significant discharge while measuring the ion beam current, the current would have fluctuated significantly and would not have been measured for a particular period. There was an unstable flow of the solution because the aqueous solution in the vacuum froze at room temperature. An 808 nm laser was irradiated to the tip of the emitter for local heating to melt it. However, without sufficient heat being transmitted, the aqueous solution can freeze and interfere with its flow. If the laser overheats the tip of the emitter, the emitter tip and the capillary tube inside the emitter may be damaged, resulting in a disrupted flow of the solution. Therefore, the laser intensity must be carefully handled and reoptimized. Despite requiring further optimization, it can still be used as a primary ion beam in its current state.

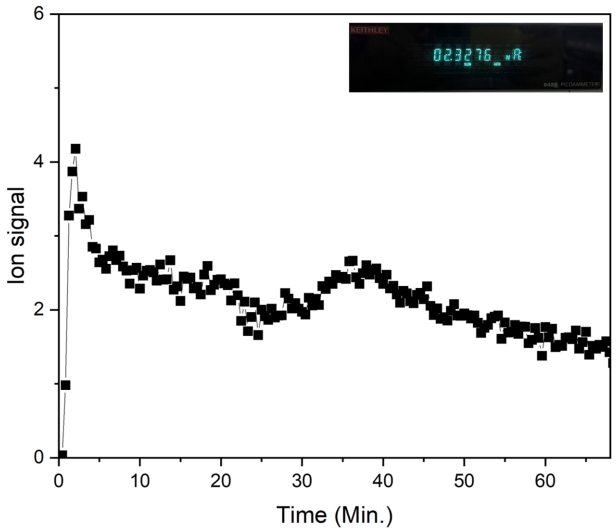

Figure 4. The current of water droplet ion beam monitored and recorded for 60 min.

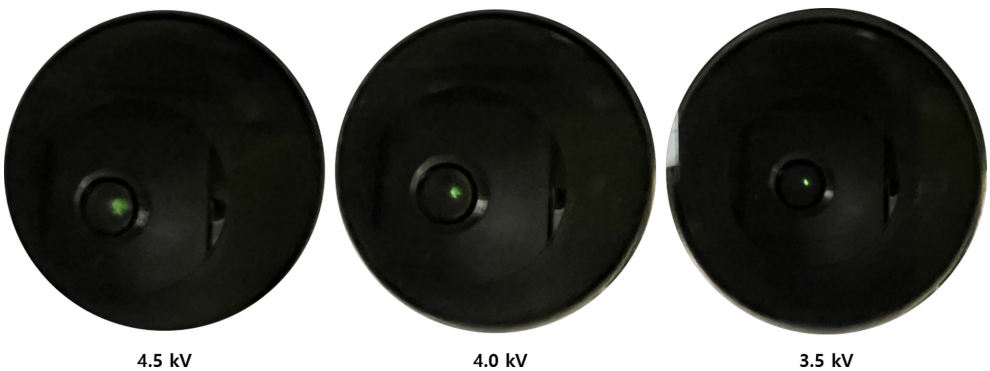

Figure 5. Photographs of the ion image on the image detector.

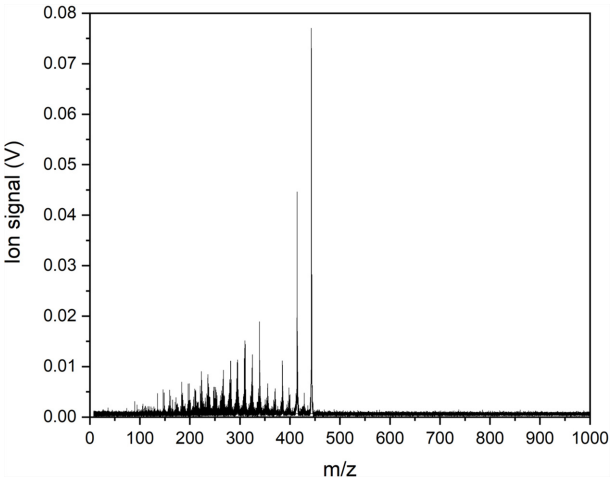

Figure 6. Secondary ion mass spectrum recorded for rhodamine 6G sputtered with a 10 keV water droplet ion projectile.

Figure 5 shows the images as a function of the voltage amplitude of the objective lens. The image detector was installed at the same height as the sample on the sample stage, as shown on the right side of Figure 2. By adjusting the voltage of the objective lens, we monitored the image from the image detector to determined the optimal conditions for reducing the size of the water-droplet ion beam. Because the diameter of one MCP channel is 12 μm, and only one MCP used, the size visible on the phosphor screen can reflect the size of the ion beam. However, the image on the phosphor screen cannot be the size of the actual ion beam. If the ion beam is sufficiently insignificant than one channel of the MCP, accurate measurement will not be possible. If the ion beam is more significant for one channel, it will be overmeasure because neighboring channels will appear as amplified signals. Therefore, the current experiment aims to optimize the objective lens of the ion beam. For future imaging mass spectrometry, imaging mass spectrometry resolution with a water droplet ion beam must be improved using grid samples with accurate distances.

Finally, the secondary ion mass spectrum of rhodamine 6G (R6G), shown in Figure 6, was sputtered with a 10 keV water droplet ion projectile. The largest peak on the right side of the spectrum was at *m/z* 443, which was the parent ion of R6G. The R6G secondary ion generated by the water droplet ion obtained a relatively intact parent ion compared to that obtained in the previous experiment. As previously reported,[24] *m/z* 415, which is the characteristic main fragment ion of R6G, was observed.

Conclusions

The field of organic molecules and biological sample analysis using secondary ion mass spectrometry (SIMS), a mass-spectrometry imaging technique, is expanding. The primary technology of SIMS for biological sample analysis is the primary ion beam, which determines how well intact organic molecules in the sample can be ionized. In this study, we generated a water droplet ion beam apparatus that can effortlessly ionize organic biomolecules and confirmed its performance for use in ToF-SIMS analysis. A current of approximately 2 nA for the ion beam, its stability, and the shape of the beam were characterized. Finally, the mass spectrum of the R6G ion, a representative organic dye molecule, produced from the thin film was obtained using ToF-SIMS in combination with a water droplet ion beam apparatus to confirm the possibility of its use as a primary ion beam. The water droplet ion beam device introduced here is smaller than the previously published one and has relatively less interference between other equipment such as ToFMS so it is expected to be easily applied to various ToF-SIMS. And It was designed to use the acceleration energy of the water droplet ion beam up to 20 kV. This means that it can be used as a surface analysis equipment to generate and analyze various organic molecules under more diverse conditions. In future, we plan to optimize the water droplet ion beam and apply it to mass spectrometry image analysis. Furthermore, this combined equipment will be able to produce more diverse results in organic surface analysis, which and significantly contribute to connectivity between the developed equipment and bio-mass spectrometric analysis.

Acknowledgments

This study was supported by a research grant from the Korea Basic Science Institute (D310100) and a National Research Foundation of Korea (NRF) grant funded by the Korean Government (MSIT) (No.2020R1C1C100521913).

References

1. Vaysse, P. M.; Heeren, R. M. A.; Porta, T.; Balluff, B. *Analyst* **2017**, 142, 2690-2712. https://doi.org/10.1039/c7an00565b.
2. Buchberger, A. R.; DeLaney, K.; Johnson, J.; Li, L. *Anal. Chem.* **2018**, 90, 240-265. https://doi.org/10.1021/acs.analchem.7b04733.
3. Swales, J. G.; Hamm, G.; Clench, M. R.; Goodwin, R. J. A. *Int. J. Mass Spectrom.* **2019**, 437, 99–112. https://doi.org/10.1016/j.ijms.2018.02.007.
4. Newbury, D. E.; Ritchie, N. W. M. *J. Anal. At. Spectrom.* **2013**, 28, 973–988. https://doi.org/10.1039/c3ja50026h.
5. Sarecka-Hujar, B.; Balwierz, R.; Ostrozka-Cieslik, A.; Dyja, R.; Lukowiec, D.; Jankowski, A. *J. Phys. Conf. Ser.* **2017**, 931, 0–5. https://doi.org/10.1088/1742-6596/931/1/012008.
6. Yu, L.; Li, M.; Wen, J.; Amine, K.; Lu, J. *Mater. Chem. Front.* **2021**, 5, 5186–5193. https://doi.org/10.1039/d1qm00275a.
7. Pal, R.; Sikder, A. K.; Saito, K.; Funston, A. M.; Bellare,

J. R. *Polym. Chem.* **2017**, 8, 6927–6937. https://doi.org/10.1039/c7py01459g.
8. Hachtel, J. A.; Jokisaari, J. R.; Krivanek, O. L.; Idrobo, J. C.; Klie, R. F. *Micros. Today* **2021**, 29, 36–41. https://doi.org/10.1017/s1551929520001789.
9. Eberlin, L. S.; Ferreira, C. R.; Dill, A. L.; Ifa, D. R.; Cooks, R. G. *Biochim. Biophys. Acta - Mol. Cell Biol. Lipids* **2011**, 1811, 946–960. https://doi.org/10.1016/j.bbalip.2011.05.006.
10. Kumara, P. M.; Srimany, A.; Arunan, S.; Ravikanth, G.; Shaanker, R. U.; Pradeep, T. *PLoS One* **2016**, 11, 1–14. https://doi.org/10.1371/journal.pone.0158099.
11. Tuck, M.; Grélard, F.; Blanc, L.; Desbenoit, N. *Front. Chem.* **2022**, 10(May), 1–11. https://doi.org/10.3389/fchem.2022.904688.
12. Aichler, M.; Walch, A. *Lab. Investig.* **2015**, 95, 422–431. https://doi.org/10.1038/labinvest.2014.156.
13. Ščupáková, K.; Balluff, B.; Tressler, C.; Adelaja, T.; Heeren, R. M. A.; Glunde, K.; Ertaylan, G. *Clin. Chem. Lab. Med.* **2020**, 58, 914–929. https://doi.org/10.1515/cclm-2019-0858.
14. Chehreh Chelgani, S.; Hart, B. *Miner. Eng.* **2014**, 57, 1–11. https://doi.org/10.1016/j.mineng.2013.12.001.
15. Stephan, T. *Planet. Space Sci.* **2001**, 49, 859–906. https://doi.org/10.1016/S0032-0633(01)00037-X.
16. Morrison, G. H. *Anal. Chem.* **1986**, 58, 1. https://doi.org/10.1021/ac00292a600.
17. Yamada, I.; Matsuo, J.; Toyoda, N.; Kirkpatrick, A. *Mater. Sci. Eng. R* **2001**, 34, 231–295.
18. Angerer, T. B.; Magnusson, Y.; Landberg, G.; Fletcher, J. S. *Anal. Chem.* **2016**, 88, 11946–11954. https://doi.org/10.1021/acs.analchem.6b03884.
19. Tian, H.; Sparvero, L. J.; Amoscato, A. A.; Bloom, A.; Baylr, H.; Kagan, V. E.; Winograd, N. *Anal. Chem.* **2017**, 89, 4611–4619. https://doi.org/10.1021/acs.analchem.7b00164.
20. Lee, S. J.; Hong, A.; Cho, J.; Choi, C. M.; Baek, J. Y.; Eo, J. Y.; Cha, B. J.; Byeon, W. J.; We, J. Y.; Hyun, S.; Jeon, M.; Jeon, C.; Ku, D. J.; Choi, M. C. *Appl. Surf. Sci.* **2022**, 572, 151467. https://doi.org/10.1016/j.apsusc.2021.151467.
21. Tian, H.; Sheraz Née Rabbani, S.; Vickerman, J. C.; Winograd, N. *Anal. Chem.* **2021**, 93, 7808–7814. https://doi.org/10.1021/acs.analchem.0c05210.
22. Ninomiya, S.; Sakai, Y.; Watanabe, R.; Sogou, M.; Miyayama, T.; Sakai, D.; Watanabe, K.; Chen, L. C.; Hiraoka, K. *Rapid Commun. Mass Spectrom.* **2016**, 30, 2279–2284. https://doi.org/10.1002/rcm.7703.
23. Ninomiya, S.; Sakai, Y.; Chuin Chen, L.; Hiraoka, K. *Mass Spectrom.* **2018**, 7, A0069–A0069. https://doi.org/10.5702/massspectrometry.a0069.
24. Choi, C. M.; Lee, S. J.; Baek, J. Y.; Kim, J. J.; Choi, M. C. *Appl. Surf. Sci.* **2018**, 458, 805–809.

